JOURNAL OF CATALYSIS **170,** 331–345 (1997)
ARTICLE NO. CA971786

Structure and Reactivity of Bimetallic FeIr/SiO_2 Catalysts after Reduction and during High-Pressure CO Hydrogenation

L. M. P. van Gruijthuijsen,*[,1] G. J. Howsmon,†[,2] W. N. Delgass,† D. C. Koningsberger,‡ R. A. van Santen,* and J. W. Niemantsverdriet*[,3]

*Schuit Institute of Catalysis, Eindhoven University of Technology, 5600 MB Eindhoven, The Netherlands; †School of Chemical Engineering, Purdue University, West Lafayette, Indiana 47907; and ‡Debye Institute, University of Utrecht, 3508 TB Utrecht, The Netherlands

Received February 10, 1997; revised May 16, 1997; accepted May 31, 1997

Bimetallic FeIr/SiO_2 CO hydrogenation catalysts have been studied by temperature-programmed reduction, EXAFS, Mössbauer spectroscopy, and previously also by infrared spectroscopy of adsorbed CO. We concentrate on the structure of a freshly reduced sample, which is selective for the formation of hydrocarbons from $CO + 3H_2$, and a catalyst activated during 48 h of reaction, which produces mainly methanol. The fresh sample contains iron oxide and bimetallic FeIr particles with an iron-rich surface after reduction in H_2 at 450°C. During CO hydrogenation, a part of the oxidic iron reduces and forms, together with some of the iron that is initially alloyed an iron carbide. CO adsorption on activated FeIr/SiO_2 is considerably weaker than on the freshly reduced catalyst, while the activated catalyst also possesses a much higher hydrogenation activity than the initially reduced system does. Structure models for the catalyst after reduction and during steady state CO hydrogenation at high pressure are discussed.

INTRODUCTION

An effective promoter of noble metal CO hydrogenation catalysts, iron is known to increase both the activity and selectivity for oxygenated products. This promoter effect was first reported by Bhasin *et al.* (1), who observed an increased methanol selectivity of FeRh as compared to unpromoted Rh/SiO_2, and a shift of the C_2-oxygenate selectivity towards ethanol. Fukushima *et al.* (2) reported a strong enhancement of the activity of Ir/SiO_2 and an increase of the methanol selectivity for catalysts with low Fe/Ir ratio ($\leq$0.2). An increase of the activity due to the addition of iron, although at constant methanol selectivity, was also observed for Pd/SiO_2 catalysts (3).

A previous study (4) from our laboratory shows that FeIr/SiO_2 catalysts of higher iron content (Fe/Ir $\leq$ 1) may have methanol selectivities as high as 80–85%. However, their favorable steady state activity and selectivity are only reached after an activation period on the order of 24 to 48 h. A group of related bimetallic catalysts, consisting of a noble metal (Ru, Rh, Pd, Pt, Ir) and a less noble metal (Fe, Co, Ni) in a 1 : 1 atomic ratio, shows the same behavior (5).

The structure of supported bimetallic FeM catalysts has been studied extensively (6–26), not in the least because these catalysts offer excellent opportunities for characterization with Mössbauer spectroscopy. Results of combined Mössbauer, EXAFS, XPS, TPR, and ESR studies prove the existence of a bimetallic phase in combination with unreduced iron in most freshly reduced catalysts. In addition to these phases, α-Fe (17, 18) and unalloyed Pd (18) have been observed in FePd/SiO_2 catalysts. The iron oxide phase has been proposed to be in close contact with the alloy (9–11), or to serve as an anchor for the bimetallic particles (13). Recent work by Sachtler and coworkers (23, 24) indicates that care must be taken in the interpretation of Mössbauer spectra, as the parameters of oxidic iron may be similar as those of surface iron in FeRh alloys. A similar situation has been encountered in highly dispersed metallic iron particles (27, 28). Hence, using a combination of techniques is essential for studying the surface composition of these bimetallic catalysts.

Iron catalysts are well known to convert to iron carbides in syngas reactions at low conversion levels (29, 30), while mixtures of iron oxide and carbide form at high conversions (31). CO-induced changes in structure are also known to occur in different types of supported noble metal catalysts (32–34). Nevertheless, the structure of the activated FeM/SiO_2 catalysts has not yet received much attention. Proposals for the active site in methanol synthesis over bimetallic FePd and FeIr catalysts (18, 20, 21) implicitly rest on knowledge about the freshly reduced catalyst. This is certainly not warranted in the case of 1 : 1 FeM/SiO_2 catalysts, as the results of this paper show.

The aim of the present study is to investigate the relation between the catalytic properties of FeM/SiO_2 catalysts and their structure during steady state catalysis. FeIr/SiO_2 has

[1] Present address: TNO Prins Maurits Laboratory, 2280 AA Rijswijk, The Netherlands.
[2] Present address: Exxon Research and Development Laboratory, Baton Rouge, LA 70821.
[3] Corresponding author: Fax: +31 40 245 5054; E-mail: tgtahn@chem.tue.nl.

0021-9517/97 $25.00

been chosen because it is the most active and most stable methanol synthesis catalyst of the FeM/SiO_2 family (5). In a recent letter (26) we used temperature programmed desorption of CO as monitored by infrared spectroscopy to show that Fe–Ir catalysts in their active state for methanol production adsorb CO much weaker than freshly reduced catalysts do. In addition, the activated Fe–Ir catalysts had much higher activity for the hydrogenation of ethylene in syngas, indicative for higher coverages of hydrogen on the catalyst in its active state. In this paper we describe the structure of $FeIr/SiO_2$ after reduction and after activation during high pressure $CO + H_2$ reaction, as studied by EXAFS, Mössbauer spectroscopy, and temperature programmed reduction. We refer to (35–37) for introductions to these techniques.

METHODS

Catalyst Preparation

$FeIr/SiO_2$ catalysts were prepared by incipient wetness impregnation of SiO_2 (Grace 332, 270 m^2/g, pore volume 1.6 ml/g) with a solution of $Fe(NO_3)_3 \cdot 9H_2O$ (Merck p.a.) and $IrCl_3 \cdot nH_2O$ (Johnson Matthey Chemicals, 54% Ir) in a 1 : 1 molar ratio. For Mössbauer experiments a catalyst enriched in the ^{57}Fe isotope of iron ($^{57}Fe/^{56}Fe = 0.1$) was prepared, by reducing $^{57}Fe_2O_3$ in H_2 before it was dissolved in nitric acid and used in the impregnating solution. The total metal loading of the catalysts was 5 wt%. After impregnation, the catalysts were dried in air at 110°C for 16 h.

Mössbauer Spectroscopy

The catalyst containing 10% of the total iron as ^{57}Fe was reduced in H_2 at 450°C and activated during 48 h in 40 bar H_2/CO at 270°C and subsequently was passivated at room temperature by exposure to a highly diluted O_2/N_2 flow and stored in air. A high pressure cell ($p_{max} = 8$ bar) was used for further treatments and *in situ* measurements of the catalyst. Mössbauer spectra were collected at Purdue University using an ASA S-600 constant acceleration spectrometer with a ^{57}Co-in-Rh source. The spectra were fitted with physically relevant parameters (isomer shift, quadrupole splitting, line width, hyperfine field, and absorbance) using a nonlinear minimization routine.

Isomer shifts are reported with respect to α-Fe. Spectra were corrected for iron impurities in the beryllium windows of the cell by subtraction of peaks of fixed isomer shift, line width, and absorbance. In cases where the sample was heated or cooled, the isomer shifts were allowed to fluctuate within a narrow range corresponding to a high Debye temperature iron–beryllium alloy.

Extended X-Ray Absorption Fine Structure

Fe K-edge and Ir L_3-edge EXAFS measurements were performed at EXAFS station 9.2 of the SRS, Daresbury, UK. Catalysts were reduced and passivated, or activated in syngas and passivated as described above. The samples were pressed in self-supporting wafers with absorption coefficients of 2.5 after the edge and measured at liquid nitrogen temperature after three treatments: (i) drying in helium at 110°C; (ii) *in situ* reduction in H_2 at 400°C during 1 h; (iii) *in situ* reduction at 400°C and CO adsorption at room temperature during 1 h. The passivated sample and the sample after CO adsorption were measured in helium atmosphere; the reduced catalyst was kept under hydrogen.

EXAFS data analysis was done with a combination of experimental and theoretical references. For most of the required absorber–backscatterer pairs, a reference compound with known structure was available. Pt foil, $Na_2Pt(OH)_6$, and $Ir_4(CO)_{12}$ were used as references for the Ir–Ir, Ir–O, and Ir–CO contributions in the Ir EXAFS spectra. It has been shown theoretically (38) and experimentally (39) that platinum references can be used to analyze iridium data. The Ir–Ir references were made by isolation of the first and fourth Pt–Pt shell in platinum foil after subtraction of the neighboring shells, as described by Kampers *et al.* (40). The Ir–O reference, isolated from the spectrum of $Na_2Pt(OH)_6$ in the interval $1.75 \leq k \leq 14.48$ Å^{-1}, was extended up to $k = 19$ Å^{-1} with backscattering amplitude = 0, in order to fit the spectra over a larger data range. This is allowed because the Ir–O backscattering amplitude decreases strongly as function of the electron wave number (k) and is zero at $k \gg 14$ Å^{-1}. The contributions in the Fe EXAFS spectra were fitted with shells from Ni foil and Fe-acetylacetonate. Ni foil was used, because the first and second Fe–Fe shells in Fe foil, which has a bcc structure, cannot be separated. References for the bimetallic pairs (Fe–Ir and Ir–Fe) were calculated with the program FEFF (41) using the parameters $N = 1$, $R = 2.69$ Å, $\sigma^2 = 0$, and $S_0^2 = 0.9$. For monometallic pairs, this program gives good results (42) and calculates distances with high accuracy. Calculated coordination numbers, however, are generally too low, with errors of up to 25%. These errors can be partially compensated using the many-body amplitude reduction factor (S_0^2).

CO Hydrogenation

Reactions were carried out in a stainless steel fixed-bed reactor. CO was led over a silica column at 300°C in order to decompose metal carbonyls and dried over a 4 Å molsieve. Hydrogen was dried and used without further purification. Catalyst samples (250 mg) were reduced in hydrogen at 450°C for 1 h and tested at 270°C and 40 bar in a $4N$ liters/h syngas flow ($H_2/CO = 3$). Products were analyzed by a gas chromatograph with a flame ionization detector.

Temperature Programmed Reduction

Temperature programmed reduction (TPR) of passivated catalysts was carried out as described previously (8),

using a 4% H_2-in-Ar flow. The temperature was increased linearly to 400°C at a heating rate of 5°C/min. Hydrogen consumption was measured by a thermal conductivity detector.

RESULTS

In this section we will present information about the structure of the active FeIr/SiO_2 catalyst, as derived from both *in situ* (Mössbauer and infrared spectroscopy) and "semi" *in situ* (EXAFS) experiments. In the latter, the catalyst had to be removed from the reaction environment, but was rereduced before measurement. Mössbauer spectroscopy has been used to follow the effect of this procedure. First we describe the results of a CO hydrogenation experiment which indicates that the "semi" *in situ* approach leads to relevant information about the catalyst in the active state.

CO hydrogenation. Figure 1 shows the activity of a 1 : 1 FeIr/SiO_2 catalyst for the formation of methanol and methane, which are the main reaction products of CO hydrogenation (4). Under standard reaction conditions, the conversion over a freshly reduced catalyst reaches steady state during an activation period of 48 h, after which the catalyst is stable. During the activation period, a new type of site appears to be formed which is active for the formation of methanol. No significant changes are observed with respect to the formation of hydrocarbons. Exposure to air at room temperature and renewed reduction by H_2 at 400°C, as is done in some of the characterization experiments, has no effect on the activity for methanol formation and only temporarily enhances the formation of hydrocarbons. We therefore conclude that characterizing the FeIr catalyst, after removal from the reactor and rereduction in the Mössbauer or EXAFS cells, is permissible for studying the FeIr catalyst in its active, methanol-producing state.

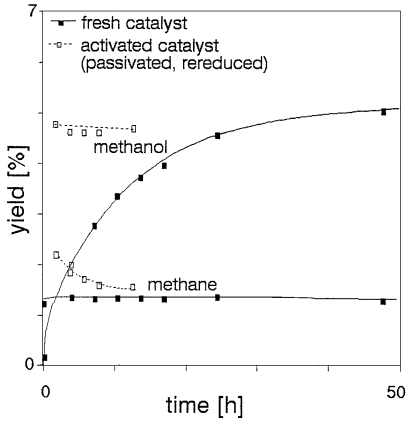

FIG. 1. Conversion of CO into methane and methanol (40 bar of $3H_2 + 1CO$ synthesis gas at 270°C). Comparison of the freshly reduced 1 : 1 FeIr/SiO_2 catalyst and the catalyst after 48 h of reaction, exposure to air at room temperature, and rereduction in H_2 at 400°C.

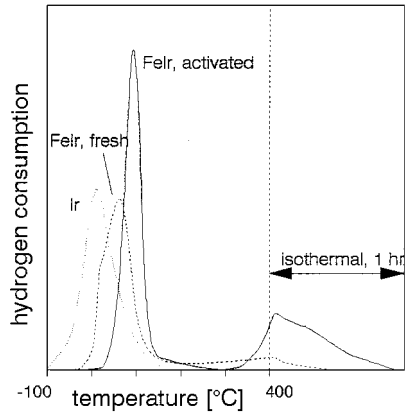

FIG. 2. Temperature programmed reduction profiles of Ir/SiO_2 and FeIr/SiO_2 catalysts. Pretreatment: reduction at 450°C and exposure to air at room temperature; activated catalyst: 48 h of reaction as in Fig. 1 followed by exposure to air at room temperature.

Temperature programmed reduction. TPR was used to study the reduction of passivated Ir/SiO_2 and 1 : 1 FeIr/SiO_2 samples. The TPR profiles of the fresh Ir and FeIr catalysts, after reduction at 450°C and oxidation at 20°C, and the activated FeIr catalyst, after 48 h of syngas reaction at 270°C and oxidation at 20°C, are shown in Fig. 2.

The Ir/SiO_2 sample reduces at low temperature, in a broad temperature interval which has its maximum at 15°C. The TPR pattern of Fe/SiO_2 (not shown) has peaks around 350°C (8, 12). Reduction of the freshly reduced and passivated FeIr/SiO_2 catalyst starts around 0°C, reaches a maximum around 60°C, and is largely completed at 120°C, although the catalyst continues to consume hydrogen during further heating to 400°C. The shift of the main peak, as compared to the TPR pattern of Ir/SiO_2, forms evidence that most of the iridium and a substantial part of the iron are well mixed. However, the catalyst also contains iron oxide that remains difficult to reduce. Mössbauer spectra, discussed in the next section, confirm that iron is indeed only partially reduced.

Reduction of the activated FeIr catalyst takes place in a single step at a temperature that is significantly higher than needed for the reduction of the fresh catalyst. In addition to this signal, a large hydrogen consumption peak arises around 400°C. Mass spectrometry experiments have shown that methane is formed at this temperature, indicating that the consumption of hydrogen at temperatures above 350°C is mainly due to the reaction with carbonaceous species formed during CO hydrogenation. Of course, we cannot exclude that part of this high temperature signal is also caused by reduction of iron oxide, as it is in the fresh catalyst.

Mössbauer spectroscopy. Figure 3 shows the ^{57}Fe Mössbauer spectra of the FeIr/SiO_2 catalyst after 48 h of CO hydrogenation in the high pressure reactor and exposure to air, after rereduction in H_2, and during and after CO

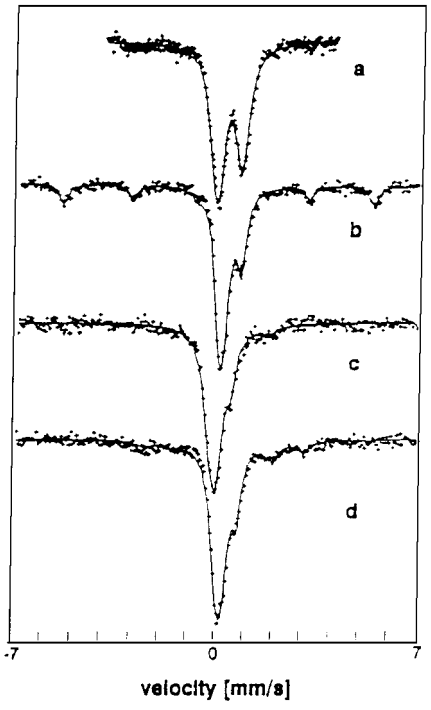

FIG. 3. Mössbauer spectra of FeIr/SiO_2 after 48 h of reaction in 40 bar of synthesis gas, after (a) passivation, (b) rereduction in H_2 at 400°C, (c) reaction in 8 bar of synthesis gas at 270°C (measured at 270°C), and (d) after reaction and cooling down to room temperature.

hydrogenation at 8 bar in the Mössbauer *in situ* cell. In order to facilitate the interpretation, spectra were recorded after cooling with liquid nitrogen to about −170°C as well. The fact that for each component the isomer shift and the resonant absorption area should increase with decreasing temperature, imposes powerful constraints on the computer fits (9). The parameters of the fits are listed in Table 1.

The spectrum of the passivated catalyst (Fig. 3a) consists predominantly of a quadrupole doublet due to Fe^{3+}, with a small contribution of a singlet corresponding to an fcc FeIr alloy. The spectrum of the reduced catalyst (Fig. 3b) shows a clear decrease in intensity of this doublet, indicating that iron oxide is reduced to Fe^0, present in an alloy (singlet at 0.17 mm/s) and in metallic iron (six-line component). The low temperature spectrum shows the same phases, but indicates also that the doublet phase exhibits the largest increase in absorption area and is thus a surface phase (see Table 1). Correcting for the relatively low Debye temperature of this phase, we estimate that approximately 50% of the iron contributes to this surface doublet and is oxidic after rereduction at 400°C. Although the parameters of this doublet are characteristic of Fe^{3+}, the work of Schuenemann *et al.* (23) indicates that we should not exclude that iron in the surface of the alloy particles contributes to this doublet as well.

The spectrum of the catalyst after CO hydrogenation in the Mössbauer reactor (Fig. 3d) indicates that a carbide phase forms from the α-Fe, and that part of the Fe^{3+} is reduced to Fe^{2+}. Conversion of Fe^{3+} to Fe^{2+} has also been observed after adsorption of CO on bimetallic FeM catalysts at room temperature (10–12). The *in situ* spectrum recorded during reaction at 270°C (Fig. 3c), only shows recognizable signals of Fe^{2+}, Fe^{3+}, and FeIr, because the signal of the carbide, which at 270°C apparently is in the superparamagnetic state, overlaps with the main peaks of FeIr and Fe^{3+}. However, at room temperature (Fig. 3d) a magnetically split signal is visible, with the Mössbauer parameters of ϵ'-$Fe_{2.2}C$. As the spectral area of the ϵ'-$Fe_{2.2}C$ signal increases only slightly after cooling to −170°C (Table 1), we conclude that no superparamagnetic carbide is present at room temperature.

In the Mössbauer spectra taken after reaction we also see that the doublet phase has a Debye temperature that is significantly lower than that of the other iron phases. We therefore conclude that the Fe^{3+} phase is highly dispersed.

The following experiments give indirect information about the relative dispersions of the iron phases in the catalyst after activation. Figure 4a shows the Mössbauer spectrum of the catalyst under hydrogen at room temperature after *in situ* reaction and cooling in synthesis gas. The spectrum does not differ significantly from that in Fig. 3d, recorded after cooling down in synthesis gas. Exposure of

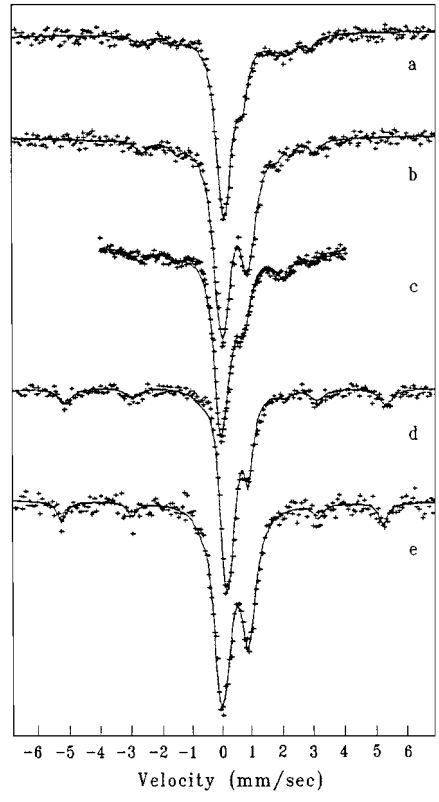

FIG. 4. Mössbauer spectra of FeIr/SiO_2, after (a) reaction under H_2, (b) exposure to 1% O_2 in He, (c) reexposure to H_2 at room temperature, (d) rereduction at 400°C, and (e) exposure to 1% O_2 in He.

TABLE 1

Mössbauer Parameters of 1 : 1 FeIr/SiO_2

Experimental conditions	T (°C)	Iron species	IS (mm/s)	QS (mm/s)	H (kOe)	LW (mm/s)	Area a.u.	(%)
Passivated	20	Fe^{3+}	0.37	0.93	—	0.56	4.14	88
		FeIr	0.10	—	—	0.33	0.57	12
Reduced	20	Fe^0	0.02	0.00	332	0.38	1.13	21
		$Fe^{3+} + Fe^0_{surf}$	0.38	0.80	—	0.35	1.68	31
		FeIr	0.17	—	—	0.51	2.68	48
	−173	Fe^0	0.13	0.00	341	0.43	1.41	16
		$Fe^{3+} + Fe^0_{surf}$	0.52	0.88	—	0.54	3.76	42
		FeIr	0.24	—	—	0.59	3.88	42
8 bar H_2/CO	270	Fe^{2+}	1.00	1.65	—	0.54	0.22	7
		$Fe^{3+} + Fe^0_{surf}$	0.14	0.84	—	0.38	0.69	23
		FeIr	0.01	—	—	0.60	2.06	70
Post reaction	20	Fe^{2+}	1.21	1.64	—	0.46	0.42	8
		$Fe^{3+} + Fe^0_{surf}$	0.35	0.78	—	0.35	1.39	25
		ϵ'-$Fe_{2.2}C$	0.19	0.03	176	0.55	0.72	13
		FeIr	0.15	—	—	0.57	2.99	54
	−173	Fe^{2+}	1.51	1.90	—	0.58	0.65	7
		$Fe^{3+} + Fe^0_{surf}$	0.46	0.84	—	0.46	2.68	32
		ϵ'-$Fe_{2.2}C$	0.30	0.01	186	0.63	0.82	10
		FeIr	0.24	—	—	0.61	4.33	51
1% O_2/He, 20°C	20	Fe^{2+}	1.30	1.86	—	0.46	0.13	2
		Fe^{3+}	0.37	0.92	—	0.60	3.80	65
		ϵ'-$Fe_{2.2}C$	0.19	0.03	176	0.55	0.65	11
		FeIr	0.15	—	—	0.47	1.26	22
H_2 at 20°C	20	Fe^{2+}	1.26	1.74	—	0.46	0.70	12
		$Fe^{3+} + Fe^0_{surf}$	0.40	0.79	—	0.46	1.74	32
		ϵ'-$Fe_{2.2}C$	0.19	0.03	176	0.55	0.72	13
		FeIr	0.11	—	—	0.57	2.36	43
H_2 at 400°C	20	Fe^{2+}	1.20	1.65	—	0.26	0.13	2
		$Fe^{3+} + Fe^0_{surf}$	0.38	0.82	—	0.34	1.67	28
		Fe^0	0.04	0.00	330	0.51	1.13	19
		FeIr	0.17	—	—	0.52	2.96	51
1% O_2/He, 20°C	20	Fe^0	0.03	0.00	331	0.37	0.87	14
		Fe^{3+}	0.38	0.94	—	0.56	3.84	61
		FeIr	0.12	—	—	0.54	1.55	25

Note. Catalyst pretreatment: 48 h of activation in 40 bar $H_2/CO = 3$ at 270°C, and passivation by exposure to air at room temperature. Accuracies: IS ± 0.02 mm/s; QS ± 0.04 mm/s; H ± 5 kOe; Area ±15%.

this catalyst to 1% O_2-in-He (Fig. 4b) leads to a strong increase in the intensity of the Fe^{3+} signal. The computer fit shows that roughly 75% of the Fe^{2+} phase, 50% of the iron in the FeIr alloy and a smaller amount (about 20%) of the iron carbide convert to Fe^{3+}. This suggests that the Fe^{2+} phase has a high dispersion, the FeIr alloy somewhat less, and the carbide phase has the lowest dispersion. The increased quadrupole splitting and line width of the Fe^{3+} component point to a less homogeneous environment of an Fe^{3+} ion in the passivated catalyst and is in qualitative agreement with the presence of Fe^{3+} at the surface of three different iron-containing phases.

Interestingly, reintroduction of hydrogen at room temperature partly reverses the effect of oxidation (Fig. 4c); a substantial fraction of the Fe^{3+} becomes reduced to Fe^{2+} and to Fe^0 in the FeIr alloy, while the intensity of the carbide does not change significantly. Reduction at the normally employed temperature of 400°C yields a Mössbauer spectrum (Fig. 4d) that is essentially identical to that of Fig. 3b. Note that the iron carbide has converted to metallic iron. Exposure of this sample to 1% of O_2-in-He at room temperature oxidizes half of the iron in the FeIr alloy and a minor part of the α-Fe particles, confirming once more that the metallic iron particles are significantly larger than the FeIr particles.

The isomer shift of FeIr alloys increases almost linearly with the Ir content of the alloy (43) and can thus be used to estimate its composition. The isomer shift values of the

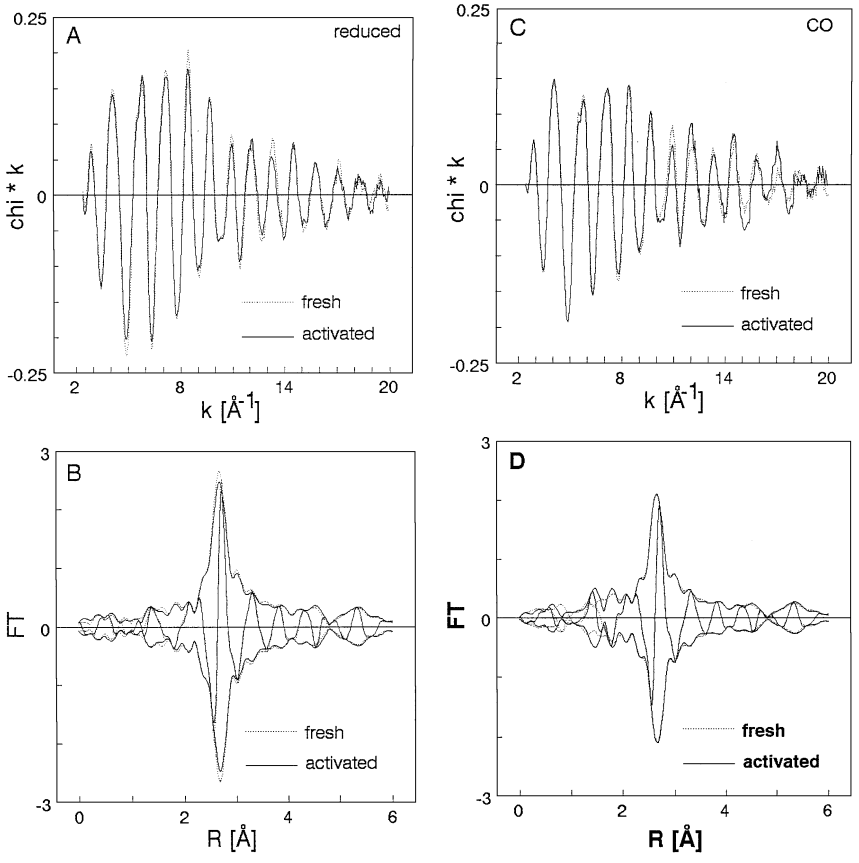

FIG. 5. Iridium L_{III}-edge EXAFS spectra (k^1-weighted) and Fourier transforms of fresh and activated $FeIr/SiO_2$ catalysts after reduction (A, B), CO adsorption (C, D), and passivation (E, F). The k^1-weighted Fourier transforms have been corrected for phase and amplitude (Pt–Pt), and they have been obtained over the ranges $k = 3.73$–16.70 Å^{-1} (B, D) and $k = 3.30$–16.70 Å^{-1} (F).

FeIr phase in Table 1 all point to alloys which are rich in iridium. More detailed conclusions on the composition of the alloy are not warranted in view of the uncertainties of the fitted parameters as shown in Table 1.

EXAFS. Iridium L_{III}- and iron K-edge EXAFS spectra have been measured of the fresh $FeIr/SiO_2$ catalyst, which produces mainly hydrocarbons, and the activated catalyst after 48 h syngas reaction, which is active and selective for the formation of methanol. Limitations set by the capabilities of the EXAFS *in situ* cell, which is unsuitable for high pressure catalytic reactions, dictated that, in contrast to the Mössbauer experiments, the catalyst could not be measured during or after *in situ* reaction. The main objective of this EXAFS study is therefore to determine the structure of the fresh and activated catalyst after reduction, since this represents conditions as close to the active state as we can achieve. We discuss EXAFS spectra of the fresh and spent catalysts and of the samples after CO adsorption at room temperature. These additional measurements appear informative about the homogeneity of the bimetallic phase in the reduced system.

Iridium L_{III}-Edge

Figure 5 shows the k^1-weighted Ir EXAFS spectra and the k^1-weighted Pt–Pt phase and amplitude corrected Fourier transforms of the fresh and activated sample after the three pretreatments (reduced: Figs. 5A, B; CO adsorption at room temperature: Figs. 5C, D; passivation: Figs. 5E, F). The quality of the data up to $k = 17$ Å^{-1} is good (Figs. 5A, C, E). The standard deviations per data point, as determined by averaging of multiple spectra and from the noise at high k-values, are between 5×10^{-4} for the reduced catalyst and 10^{-3} for the passivated sample. It is obvious from the raw data that for each pretreatment the differences between the iridium in the fresh and activated sample, as determined with EXAFS, are small. In all cases the phase of the EXAFS oscillations is similar and the differences in amplitude are small (Figs. 5A, C, E). However, the effects of different pretreatments (reduction, CO adsorption, and passivation) on the catalyst structure are much larger, as is most clearly revealed by comparing the Fourier transformed spectra of Figs. 5B, D, and F. Since the Fourier transforms of the different spectra are taken over almost the same k-range and are plotted on the same vertical scale, a direct comparison

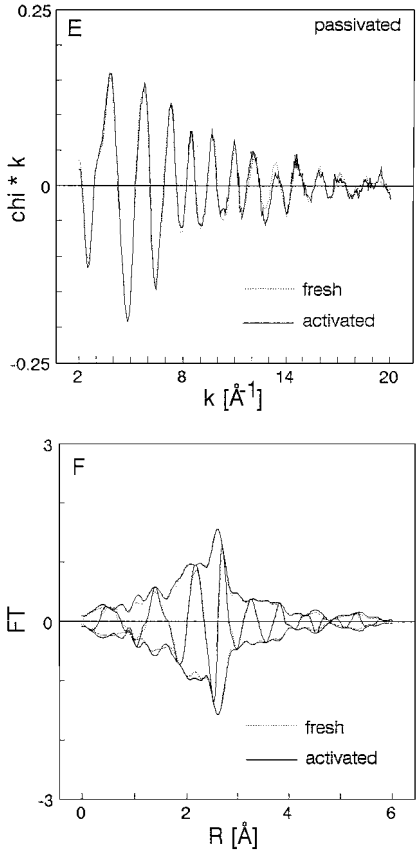

FIG. 5—*Continued*

shows that the amplitudes of the Fourier transform decrease in the order: *reduction* > *CO chemisorption* > *passivation*.

The spectrum of the reduced catalyst consists of a main peak at 2.7 Å due to first shell Ir-metal contributions, and smaller Ir-metal peaks at higher shell distances. The visible asymmetry in both the magnitude and the imaginary parts of the (Pt–Pt phase and amplitude corrected) first shell peak indicates that not only an Ir–Ir contribution, but also another scatterer like iron and/or oxygen are present. The presence of the higher Ir-metal contributions indicates that these particles are relatively large.

In a first attempt to fit the spectrum with the least number of free parameters, we tried to fit the Ir EXAFS of Fig. 5A with a combination of Ir–Ir and Ir–Fe shells only. Iridium and iron are detected at 2.69 and 2.62 Å, and also at distances of approximately $\sqrt{2}$ and $\sqrt{3}$ times the first-shell distance. However, the higher shell coordination numbers as found in this fit were much too small, indicating that the chosen model cannot be correct.

The spectrum is better described by including an Ir–O interaction (Table 2, Fig. 6). In terms of data analysis, addition of an Ir–O contribution causes an increased amplitude of the EXAFS at low *k*-value, since the backscattering amplitude of oxygen has its maximum in this region. In order to fit the spectrum at high *k*-values where oxygen has no

TABLE 2

Ir EXAFS of the Fresh FeIr/SiO_2 Catalyst after Reduction

	N_C[a]	$\Delta\sigma^2$ (Å^2)	R (Å)	E_0 (eV)
Ir–Ir	6.5	0.0012	2.696	4.2
	3.4	0.0032	3.780	8.5
	8.8	0.0046	4.692	−9.5
	2.7	0.0022	5.378	5.2
Ir–Fe	2.7	0.0052	2.639	−11
	0.8	0.0021	3.692	−11
	5.7	0.0076	4.642	−3.3
Ir–O	0.7	0.0030	2.266	−19

Note. Estimated accuracy of the first shell parameters of Ir–Ir, Ir–O: N, $\Delta\sigma^2$, E_0 ± 20%; R ± 1%. Higher shells Ir–Ir: N, $\Delta\sigma^2$ ± 30%; E_0 ± 20%; R ± 1%. First shell Ir–Fe: N, $\Delta\sigma^2$ ± 30%; E_0 ± 20%; R ± 1%. Higher shells Ir–Fe: N, $\Delta\sigma^2$ ± 40%, E_0 ± 20%; R ± 1%.

[a] Corrected with $\lambda = 8$ Å.

influence, N and $\Delta\sigma^2$ in the iridium-metal shells have to be decreased. When this procedure is used in the opposite direction; i.e., first decrease the Ir–Ir and Ir–Fe contributions and then fit the remaining part, an Ir–O contribution at 2.27 Å with a coordination number of 0.7 is detected. This

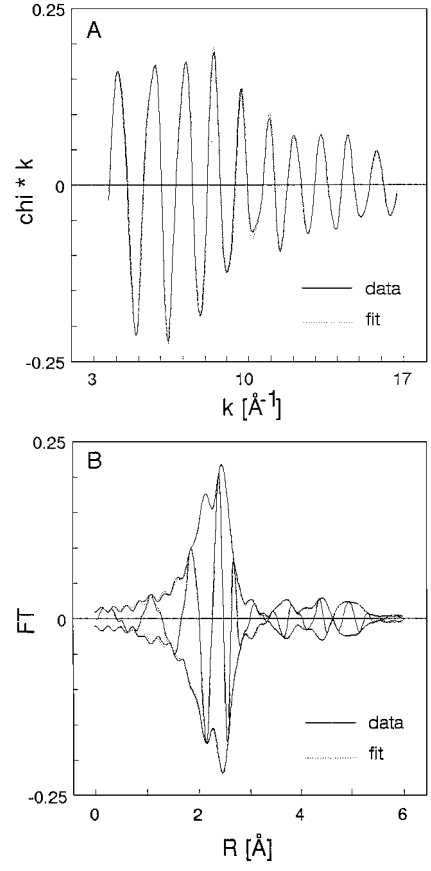

FIG. 6. Ir EXAFS of the freshly reduced FeIr/SiO_2 catalyst; solid line: Fourier filtered data (Δk: 3.7–16.7 A^{-1}; ΔR: 0.9–3.7 Å); dotted line: fit corresponding to the parameters of Table 1.

contribution can be assigned to an interaction of reduced iridium with oxygen in the support or in iron oxide. The low value of E_0 (−19 eV) has been observed previously for metal–support interactions (45) and is most likely due to differences in oxidation state between the metal in the reference compound and in the sample. In this case, first shell Ir–Ir and Ir–Fe coordination numbers of 6.5 and 2.7 are observed (Table 2), which are in much better agreement with the higher shell coordination numbers than the previous model. For all Ir EXAFS spectra, data analysis has therefore been performed according to the procedure described above (including higher coordination shells). The first-shell parameters are presented in Table 3.

The spectra of the catalyst after CO adsorption (Fig. 5D) contain the contributions that already were present after reduction, but with an about 20% lower amplitude. This indicates that CO adsorption is corrosive and affects the structure of the catalyst. Data analysis shows that the Ir–Ir and Ir–Fe coordination numbers in the fresh catalyst decrease from 6.5 to 6.0 and from 2.7 to 2.1, respectively. A similar effect is observed in the activated catalyst. The Ir–O coordination numbers in both catalysts decrease by approximately the same factor as the Ir-metal contributions. Moreover, a small decrease of the Ir–O bond length is observed. An Ir–CO contribution may be present, but has not been included in the fit because the parameters that are found for this contribution are significantly influenced by small variations in the other shells. We estimate that the Ir–CO coordination number is at most 0.3, which is not unlikely for metal particles of this size. Small differences, possibly related to the presence of carbon, exist between the fresh and activated catalyst in the region <2 Å. Similar to the Ir–CO contributions, these differences have not been determined quantitatively.

TABLE 3

Ir and Fe EXAFS of $FeIr/SiO_2$ Catalysts

	Fresh catalyst				Activated catalyst			
	N	$\Delta\sigma^2$ (Å^2)	R (Å)	E_0 (eV)	N	$\Delta\sigma^2$ (Å^2)	R (Å)	E_0 (eV)
Catalyst after reduction								
Ir–Ir	6.5	0.0012	2.696	4.2	6.2	0.0013	2.697	4.5
Ir–Fe	2.7	0.0052	2.639	−11	2.5	0.0049	2.629	−9.8
Ir–O	0.7	0.0030	2.266	−19	0.6	0.0030	2.239	−19
Fe–O	2.6	0.0095	2.005	1.5				
Fe–Ir	3.1	0.0081	2.636	−2.8	Not fully analyzed			
Fe–Fe	1.0	0.0003	2.618	4.2	Bcc Fe present			
After CO adsorption								
Ir–Ir	6.0	0.0018	2.690	4.9	5.8	0.0014	2.689	5.2
Ir–Fe	2.1	0.0071	2.632	−7.5	2.3	0.0083	2.623	−7.0
Ir–O	0.6	0.0030	2.226	−19	0.5	0.0030	2.224	−19
After passivation								
Ir–Ir	5.3	0.0019	2.668	6.1	5.4	0.0029	2.672	5.7
Ir–Fe	1.4	0.0090	2.655	−14	1.3	0.0094	2.656	−15
Ir–O	2.1	0.0017	2.046	6.3	2.2	0.0019	2.037	6.7
Fe–O	5.7	0.011	1.970	−1.8	5.0	0.012	1.985	−4.3
Fe–Fe	1.8	0.005	2.950	11	1.3	0.002	2.656	−4.5

Note. First-shell parameters. Estimated accuracy of the first shell parameters of Ir–Ir, Ir–O, Fe–Fe, Fe–O: N, $\Delta\sigma^2$, $E_0 \pm 20\%$; $R \pm 1\%$. Ir–Fe, Fe–Ir: N, $\Delta\sigma^2 \pm 30\%$; $E_0 \pm 20\%$; $R \pm 1\%$.

Passivation of the catalysts by exposure to air at room temperature has a large influence on the structure. The Fourier transformed Ir EXAFS spectrum of the passivated fresh catalyst in Fig. 5F is characterized by a much lower (about 40% less) intensity of the 2.7 Å peak, as compared to the reduced catalyst (Fig. 5B), and a significantly higher signal at 2 Å, characteristic for the Ir–O distance in an oxide. From this spectrum it is clear that both a reduced and an oxidic phase are present. The main peaks can be fitted with an Ir–O contribution at 2.05 Å, Ir–Fe at 2.66 Å, and Ir–Ir at 2.67 Å (Table 3). The Ir–O contribution at 2.26 Å in the reduced catalyst that was assigned to an interaction between the bimetallic phase and the support, is not present after passivation.

Passivation appears to have affected mainly the iron in the bimetallic phase. The first shell Ir–Fe coordination number is approximately 50% lower than after reduction (1.4 vs 2.7), whereas the Ir–Ir coordination number has decreased by only 20%. Note that coordination numbers in EXAFS are averaged over all phases, and must thus be corrected when different phases are present. The coordination numbers in Table 3 are correct only if the Ir–O and Ir-metal contributions are due to one phase. However, if we assume that the catalyst contains separate reduced and oxidic phases, and that the real Ir–O coordination number is 6, one can easily calculate that approximately 35% of the iridium is in the oxidic state. The real Ir-metal coordination number in this case is 10. Therefore, the metal particle size as determined by EXAFS is between 12 Å ($N = 6.5$, as analyzed for the reduced state) and 35 Å ($N = 10$, calculated for the passivated state). We mention that transmission electron micrographs of this catalyst indicate a particle size on the order of 1.5–2 nm (44), in clear disagreement with a high first shell coordination number.

Summarizing, the iridium EXAFS results do not reveal significant differences in catalyst structure between the reduced and passivated state.

Iron K-Edge

The k^1-weighted Fe EXAFS spectra and k^1-weighted Fe–O phase corrected Fourier transforms are shown in Fig. 7. The differences between the Fe EXAFS spectra of the fresh and activated sample after the various treatments, are much larger than the differences observed in the Ir EXAFS. However, interpretation of these differences is more complicated because only a small data range can be used ($k \leq 10$ Å^{-1}), as the spectra contain more noise. In particular in the spectra of the passivated catalysts, where

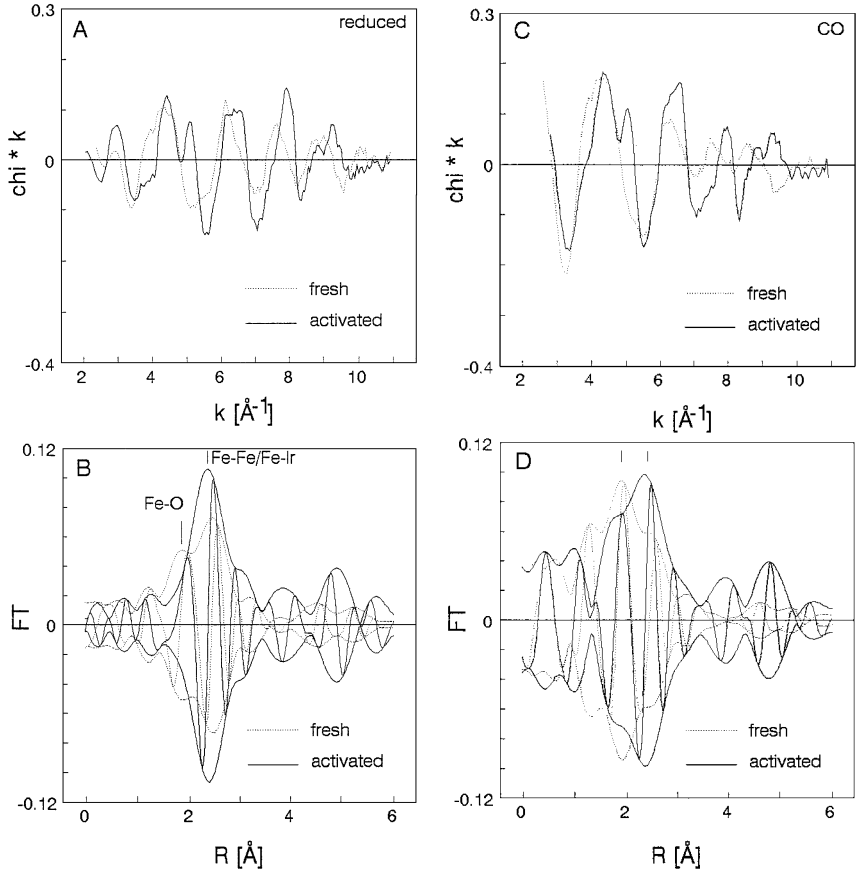

FIG. 7. Iron K-edge EXAFS spectra (k^1-weighted) and Fourier transforms of fresh and activated $FeIr/SiO_2$ catalysts after reduction (A, B), CO adsorption (C, D), and passivation (E, F).

the signal intensity decreases rapidly, noise dominates at higher k-values. Standard deviations per data point are between 2×10^{-3} for the reduced catalyst and 3×10^{-3} for the passivated catalyst. The phase and amplitude of the Fe EXAFS spectra of the fresh and activated reduced catalyst (Figs. 7A, B) are different. This shows that the activated sample contains iron in a different phase than in the fresh sample. The Fourier transformed spectrum of the freshly reduced catalyst shows a peak at 2 Å, due to the Fe–O contribution, and a peak at higher distance due to Fe-metal contributions (Fe–Fe and Fe–Ir) in the bimetallic phase. In the spectrum of the activated catalyst, the intensity of the Fe–O peak is lower, indicative of a smaller amount of oxidic iron in this catalyst, and large Fe-metal contributions at various distances are observed.

The Fe EXAFS spectrum of the reduced fresh catalyst (Figs. 7A, B) has only been partially fitted. The contributions present in the filtered EXAFS have been fitted assuming that an Fe^{3+}–Fe^{3+} interaction, observed in the passivated catalyst as will be shown later, is not present after reduction. The Fe–Ir parameters that are thus determined, are in good agreement with the fit of the Ir EXAFS data. The iron in the bimetallic phase is mostly coordinated to iridium ($N = 3$, $R = 2.64$ Å), but an Fe–Fe interaction due to iron pairs or islands in the alloy ($N = 1$, $R = 2.62$ Å) is also present. The peaks at larger distances in this spectrum are also due to Fe-metal interactions. However, these cannot be fitted with any significance because the required number of free parameters is too high. Figure 8 shows the raw EXAFS spectrum and the first shell fit.

The spectrum of the activated catalyst was not analyzed in detail, because this requires even more parameters than needed for the fit of the fresh catalyst. The nature of the new phase, however, can easily be seen in Fig. 9. In Fig. 9A we compare the spectra of the reduced fresh catalyst and the catalyst after reaction. A clear difference is observed between the phase of the oscillations in the two spectra. These differences disappear when the spectrum of an Fe foil, with a scaling factor of 0.25, is added to the spectrum of the fresh catalyst (Fig. 9B). This shows that the activated catalyst contains not only FeIr alloy and iron oxide, but also metallic iron. The iron metal is most likely formed from the iron oxide that was present after reduction, since the intensity of the Fe–O peak in the Fourier transformed spectrum (Fig. 7B) is lower. We stress again that the activated catalyst was measured after passivation and rereduction, and

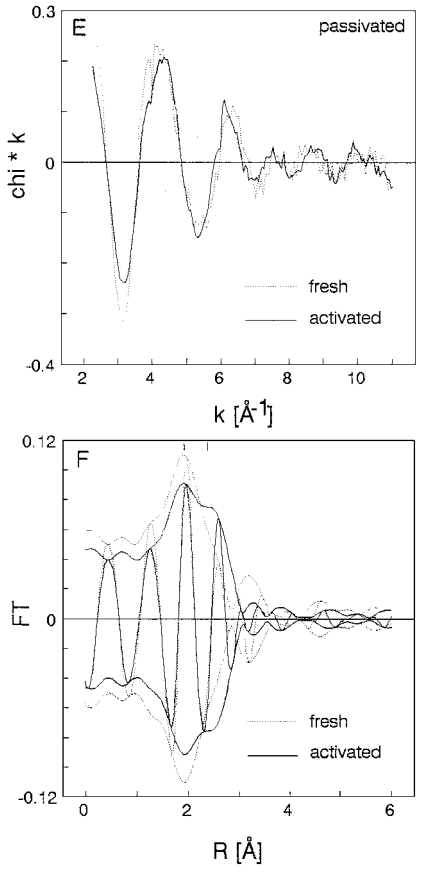

FIG. 7—*Continued*

that the metallic iron is not present as such during reaction. Indeed, the Mössbauer results discussed in the previous section confirm that the active catalyst contains iron carbide.

Only a qualitative description can be given of the changes that are observed in the Fe EXAFS spectra after adsorption of CO (Figs. 7C, D). The Fourier transform of the fresh catalyst shows a decreased intensity in the 2.5 Å region and an increased amplitude near 2 Å, as compared to the reduced catalyst. The lower intensity at 2.5 Å, where Fe-metal contributions are present, is in agreement with the decreased Ir–Fe coordination number that was found in the analysis of the iridium edge data and confirms that CO adsorption on the bimetallic phase is corrosive. The changes near 2 Å indicate an increase of the coordination of oxygen or carbon around iron. It is not possible to distinguish between these two low-Z scatterers which give similar phase shift and backscattering amplitude. We can, however, exclude that the peak is due to molecularly adsorbed CO, as this should also give a characteristic peak at 3 Å due to the carbonyl oxygen atom. The changes in the activated catalyst appear similar to those in the fresh sample. An increase of the Fe–O or Fe–C signal is also observed in the spectrum of this catalyst. The metallic iron, however, is not influenced by CO.

The Fe EXAFS spectrum of the passivated fresh catalyst (Figs. 7E, F) contains contributions of Fe–O and Fe–Fe shells. The main peak in the Fourier transformed spectrum is due to an Fe–O interaction in iron oxide at an average distance of 1.97 Å (Table 3). The high Debye–Waller factor of this shell indicates that the oxide is highly disordered. In addition to Fe–O, an Fe–Fe contribution at 2.95 Å is required to fit the spectrum. We assign this shell to Fe^{3+}–Fe^{3+} pairs in the oxide. The Fe–Ir interaction that was observed in the Ir EXAFS spectra is not discerned in the Fe spectrum.

After reaction the amount of oxide in the passivated catalyst is lower, as is shown by the decrease of the Fe–O coordination number from 5.9 to 4.9. The Fe^{3+}–Fe^{3+} shell of the fresh catalyst is no longer present, but a new Fe–Fe distance is detected ($R = 2.65$ Å), which we assign to iron in an fcc phase.

DISCUSSION

An important conclusion from this work is that a bimetallic $FeIr/SiO_2$ catalyst, which represents a class of bimetallic catalysts consisting of nonnoble and noble Group VIII

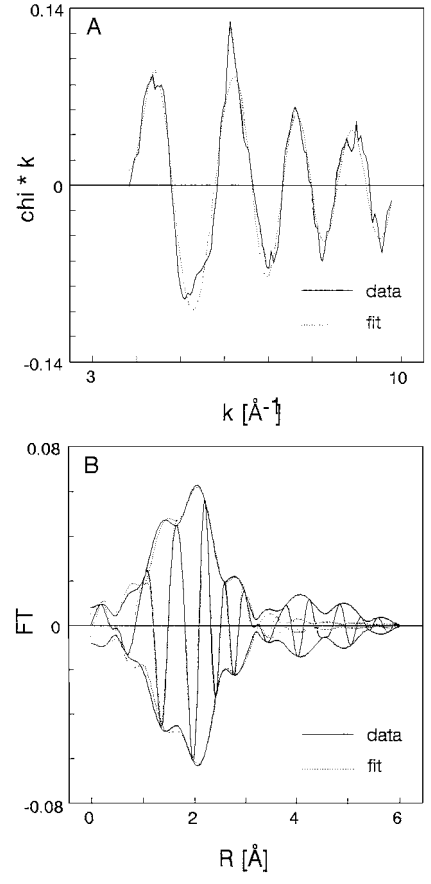

FIG. 8. Iron K-edge EXAFS spectrum (k^1-weighted) and Fourier transforms of freshly reduced $FeIr/SiO_2$, together with the first-shell fit corresponding to the parameters of Table 3. Fourier filtering: Δk: 3.7–9.9 $Å^{-1}$; ΔR: 0.5–3.2 Å.

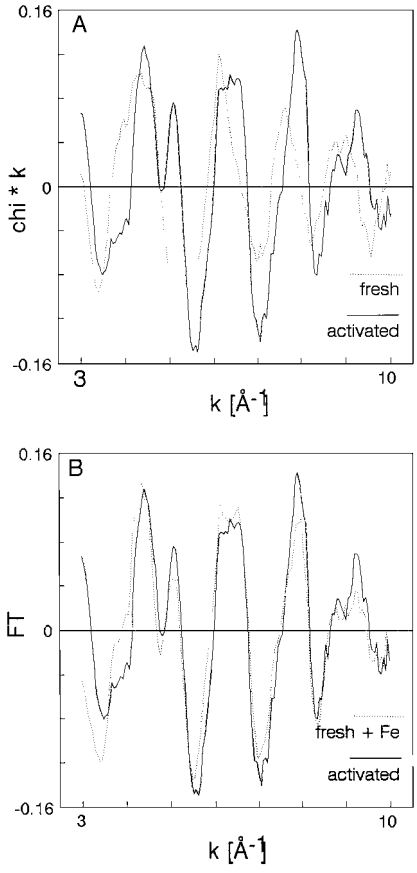

FIG. 9. Iron K-edge EXAFS spectrum (k^1-weighted) of fresh and activated $FeIr/SiO_2$ (left) and comparison of the spectrum of the activated catalyst (dotted line) with a linear combination of the spectrum of the reduced catalyst and that of an α-Fe foil (scaling factor for the Fe foil: 0.25).

metals, exhibits striking changes both in structure and in surface reactivity when used in high pressure CO hydrogenation. Commonly, characterization studies, also from our laboratories, have concerned the freshly reduced state of the bimetallic catalyst, which represents its state at the start of the catalytic reaction. The present results clearly show that if one attempts to correlate catalytic behavior under steady state reaction conditions with the structure of a catalyst, the latter must as much as possible be representative of the working catalyst. In the following we will first discuss the structure of the freshly reduced FeIr catalyst and that of the catalyst during reaction. Next we discuss the changes in reactivity of the catalytic surfaces.

Models for the structure of bimetallic catalysts have been proposed in literature, mostly based on results of Mössbauer experiments. The models can be divided in two types, which assume either full reduction of the metal (6), or the presence of an iron oxide phase in addition to an alloy (7–22); incidentally, unalloyed metals may be present as has been observed in $FePd/SiO_2$ (17, 18).

In the former model (6), a doublet present in the Mössbauer spectra of reduced FeM/SiO_2 catalysts was assigned to Fe^0 in a surface alloy phase (Fig. 10d). Indeed, recent work by Schuenemann *et al.* (23) confirms that zerovalent iron in the surface of FeRh alloys can have a similar isomer shift and quadrupole splitting as high-spin trivalent iron has. However, several studies have shown that at least a substantial part of the doublet should be assigned to Fe^{3+} (9–12, 14). Niemantsverdriet *et al.* (11) discuss three possible arrangements (Figs. 10a–c) for a bimetallic phase in close contact with highly dispersed iron oxide. These models are in agreement with the Mössbauer spectra, and explain the observed behavior of the catalyst under CO, i.e. the reduction of part of the Fe^{3+} to Fe^{2+}. Reduction of Fe^{3+} by CO would be difficult to explain by model e, where iron oxide is not accessible to CO. Kannan *et al.* (22) propose that the Fe^{3+} in $FeRu/SiO_2$ catalysts arises from the oxidation of highly dispersed iron particles on the support, which would be in agreement with the model in Fig. 10f.

From the results of an EXAFS study of $FeRh/SiO_2$, Ichikawa *et al.* (13) conclude that bimetallic particles are anchored to the support by iron oxide, e.g. as in model a or b. Their catalyst had an average particle size of about 2.5 nm, i.e. similar to the catalyst used in the present study. Catalysts derived from bimetallic carbonyl clusters contain significantly smaller metal particles, but these sinter to 20 Å in the presence of CO (21).

Here we address the structure of the fresh $FeIr/SiO_2$ catalyst on the basis of our EXAFS results and compare our findings with previous Mössbauer studies. Relevant information about the catalyst structure is obtained from the EXAFS spectra after three different pretreatments:

- Spectra of the catalyst after reduction measured under H_2 give direct information on the composition, dispersion, and interaction between the metal and oxides;
- Spectra of the passivated sample give additional information about the structure of the bimetallic phase in the reduced system, in particular about the homogeneity of the alloy;
- CO adsorption experiments show that CO influences the catalyst structure.

Catalyst after Reduction

The EXAFS parameters (Table 2) show the presence of a bimetallic phase and iron oxide in the reduced catalyst,

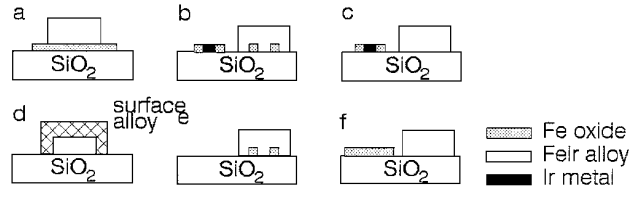

FIG. 10. Several models proposed for the structure of freshly reduced, iron-containing bimetallic catalysts consisting of iron and a noble group-8 metal, after Niemantsverdriet *et al.* (11).

in agreement with the results of previous Mössbauer studies. Interactions between iridium and iron, which prove the existence of a bimetallic phase, are clearly distinguished in both the Fe and the Ir EXAFS spectra, which both contain an Fe–Ir contribution with a distance of 2.64 Å and a coordination number of 3. In addition to these bimetallic pairs, the spectra contain an Fe–Fe contribution at 2.61 Å ($N = 1$) and an Ir–Ir shell at 2.70 Å ($N = 6.5$). Because the TPR profile of the passivated fresh catalyst (Fig. 2) shows no significant amount of unalloyed iridium, we attribute all these shells to interactions in the bimetallic phase. The total coordination number in the bimetallic phase is 10.5, which points to a metal particle size of approximately 3 nm.

The presence of an iron oxide phase in the reduced catalyst follows from the Fe–O contribution at 2.0 Å in the Fe EXAFS spectrum. The fraction of iron in the oxide may be calculated from the experimental (fractional) Fe–O coordination numbers, provided that the real coordination around iron is known. Assuming a real coordination number between 4 and 6, the experimental Fe–O coordination number of 2.6 ± 0.5 shows that 50 ± 15% of the iron is oxidic. This is in reasonable agreement with Mössbauer studies of similarly prepared catalysts, where 50–75% oxidic iron was detected (11, 12).

The EXAFS data of the reduced catalyst alone are insufficiently discriminative to confirm or reject any of the arrangements in Fig. 10. We can be more definitive when the data of the catalysts after all treatments are taken into account, as discussed later on.

Passivation

The EXAFS spectra of the passivated catalyst contain contributions of oxidic and reduced phases (Table 3). The Ir EXAFS spectrum is described by the same Ir–Ir and Ir–Fe contributions that are present in the spectrum of the reduced catalyst, although with different coordination numbers, and two Ir–O shells that we assign to iridium oxide. This assignment may at first sight be in contradiction with previous XPS results (11, 12), which indicated that the noble metal in passivated FeM/SiO_2 catalysts remained in the reduced state. It appears now, however, that this conclusion was not correct. During XPS measurement, the sample heats up due to the proximity of the hot X-ray source. This may have caused the decomposition of any noble metal oxide species in the catalysts. We have verified by using monochromatic XPS, where the X-ray source is at a large distance from the sample and heating of the latter is thus prevented, that a passivated FeIr/SiO_2 catalyst contains iridium oxide, in agreement with the EXAFS results.

The presence of Ir–Fe contributions in the Ir EXAFS proves that the reduced particles in the passivated catalyst are at least in part bimetallic, in agreement with Mössbauer spectra of passivated FeIr/SiO_2, which also show that a minor fraction of the iron remains present in an FeIr alloy (12). The Fe EXAFS consists of a disordered Fe–O shell at 1.97 Å and an Fe–Fe contribution at 2.95 Å, which indicates that iron is mostly oxidized. The Ir EXAFS spectrum cannot be fitted with physically relevant parameters, however, without including the Ir–Fe^0 shells. The relatively high Debye–Waller factor of the Ir–Ir and Ir–Fe contributions, as compared to the reduced catalyst (Table 3), indicates a static disorder which may be the result of a varying bond length from the inside of the metal particle to the surface layer. The surface of the bimetallic particles obviously is covered by an oxidic layer that contains both iridium and iron, as suggested by the TPR results in Fig. 2.

In comparison to the reduced catalyst, all coordination numbers of the bimetallic phase in the passivated sample are lower: the first shell Ir–Ir coordination number has decreased from 6.5 to 5.3, Ir–Fe from 2.7 to 1.4, and Fe–Fe from 1.0 to 0. The preferential oxidation of iron, following from the fact that the Ir–Fe and Fe–Fe coordination numbers decrease more than that of the Ir–Ir contribution, suggests that iron was mainly present at the surface of the FeIr particles after reduction. Although oxygen-induced segregation of iron may to some extent be responsible for the observed effects, we think that the bimetallic phase is inhomogeneous and should be described as a core enriched in iridium and an iron-rich surface.

CO Adsorption

The Fe EXAFS spectrum of the reduced catalyst after CO adsorption only gives qualitative information about the catalyst structure. As compared to the catalyst after reduction, the spectrum appears to contain smaller Fe–Fe and Fe–Ir contributions and a larger contribution due to an Fe–C or Fe–O interaction (Fig. 7D). An important observation in the Ir EXAFS spectrum is the decrease of the coordination number as indicated by the lower amplitude of Fig. 5D, as compared to Fig. 5B. Data analysis shows a decrease of the Ir–Fe coordination number from 2.7 after reduction to 2.1 after CO adsorption, and a decrease of the Ir–Ir coordination from 6.5 to 6.0. The relatively stronger decrease of the Ir–Fe coordination number confirms the enrichment of the surface by iron, as also concluded from the spectra after passivation. Moreover, the decrease of the coordination numbers indicates that the bimetallic phase is not stable in presence of CO, which may be a first step toward changes that occur during $CO + H_2$ reaction. As the sensitivity of EXAFS for changes at the surface is relatively low, due to the presence of relatively large metal particles and the combination of low-, medium-, and high-Z scatterers, it is not possible to derive more precise information.

Thus, the EXAFS results support the conclusions from Mössbauer spectroscopy that the freshly reduced FeIr catalysts consist of iron oxide and a bimetallic phase. Combining EXAFS results obtained after reduction, passivation, and CO adsorption enables a refinement of the models

proposed on the basis of previous Mössbauer investigations. The Ir EXAFS spectrum of the catalyst after reduction is difficult to reconcile with the model of Fig. 10a, in which the bimetallic phase partially covers a layer of iron oxide. The bimetallic phase may be anchored by small particles of iron oxide (Fig. 10b), or by oxidic iron in the interface between bimetallic phase and the support. The bimetallic phase appears to be inhomogeneous, having particles with a core enriched in iridium, and a surface enriched in iron. Ironically, the model that we arrive at is similar to the previously rejected (11) surface alloy model (Fig. 10d), which was based on incorrectly interpreted Mössbauer spectra. We stress that in addition to the Fe–Ir alloy phases shown in Fig. 10d, oxidic iron is present as in Figs. 10b, c, or f. The Ir and Fe EXAFS spectra after CO adsorption show that the structure of both the iron oxide and the bimetallic phase changes upon CO adsorption.

Structure of the activated catalyst. CO hydrogenation, EXAFS, and Mössbauer spectroscopy clearly reveal that the structure and composition of the 1 : 1 FeIr/SiO_2 catalyst changes significantly during the time that the catalyst reaches steady-state conversion conditions. Infrared spectroscopy and ethylene hydrogenation experiments reported in (26) confirm that the reactivity of the surface changes drastically as well. The main structural changes appear associated with the iron in the catalyst.

The Ir EXAFS spectra reveal only small differences in the environment of iridium between the fresh and the activated catalyst (Fig. 5). The similarity of the EXAFS spectra of the fresh and activated catalyst suggests that significant changes in the bulk structure of the bimetallic particles do not occur. We therefore exclude that the activation of the FeIr/SiO_2 catalyst is due to a *redispersion* of the alloy during the syngas reaction.

The Fourier-transformed Ir EXAFS spectra only show a small effect in the region below 2 Å, where an additional contribution appears to be present in the activated catalyst. This contribution is most likely due to an Ir–C interaction, caused by carbon deposition on the bimetallic phase. A second indication for carburization of the surface is given by the TPR profile of the passivated catalyst. After reaction an increase of the reduction temperature is observed. As mass spectroscopy confirmed the evolution of methane, we attribute the shift in reduction temperature as well as the feature in the Ir EXAFS to the presence of carbon at the metal surface.

The Fe EXAFS and Mössbauer spectra clearly show that, contrary to iridium, the local coordination around iron changes significantly during reaction. In the Mössbauer spectrum of the rereduced activated catalyst (Fig. 3b), an α-Fe phase is observed which is not present in freshly reduced samples. We propose that the high initial methanation activity of the rereduced catalyst (Fig. 1) is due to the presence of this phase. During reaction the α-Fe is converted to ϵ'-$Fe_{2.2}C$ (Fig. 3d), on which surface carbon is deposited as in monometallic iron Fischer–Tropsch catalysts, causing a decrease of the methanation activity. Comparison of the magnetic splitting of the ϵ'-$Fe_{2.2}C$ signal as a function of temperature, H(T), with data from Amelse *et al.* (46), shows that the particle size of the carbide is at least 10 nm. The EXAFS spectra of the activated catalyst after reduction and CO adsorption (Figs. 7B, D) confirm the presence of relatively large Fe particles. The metallic iron phase obviously is formed by reduction of iron oxide, as is indicated by a lower amplitude of the Fe–O contributions.

Due to the presence of the large α-Fe particles, which dominate the EXAFS, the Fe EXAFS spectra of the activated catalyst after reduction and CO adsorption give no direct information about the bimetallic phase, other than the metal particle size. Spectra obtained after passivation, however, provide useful indirect information. The spectrum of the fresh catalyst after passivation contains an Fe^{3+}–Fe^{3+} contribution, which indicates that iron in the bimetallic phase forms a bulk oxide, although of disordered structure, after oxygen adsorption at room temperature. The spectrum of the activated catalyst after passivation does not contain such an Fe^{3+}–Fe^{3+} contribution.

Evolution of the active FeIr catalyst. The yield behavior as a function of time, shown in Fig. 1, has interesting implications for the evolution or surface chemistry and active sites over the first 50 h of reaction. The activity for methane production remains essentially constant, but the methanol yield increases roughly 50-fold. Furthermore, passivation and rereduction does not destroy the methanol sites but does temporarily promote the methane sites. In considering the chemical and morphological changes in the catalyst that might account for this behavior, we must bear two additional facts in mind. First, catalysts with high Ir/Fe ratios show good methanol selectivity immediately (4), implying that the surface active for methanol is iridium-rich. Second, large iron particles go through a maximum in methane production as they carburize and then decay to low activity (29, 30) while small iron particles can have a sustained methane activity (47, 48). Furthermore, oxide formation, carbide formation, and the relative surface free energies of the metals all provide a thermodynamic driving force for segregation of iron at the surface of an Fe–Ir alloy. Thus, we can envision the following scenario to explain the kinetic behavior.

The freshly reduced catalyst has an alloy surface too rich in iron to catalyze methanol production. Any mid to large size, separated iron particles carburize and decay in activity in the first hours of reaction. A population of stabilized small particles can account for the ongoing activity for methane. Carbon deposited on the iron-rich alloy will continue to draw iron to the surface until the iron carbon layer is sufficiently thick to nucleate iron carbide. If this carbide grows in a three-dimensional structure, i.e. particle or

crystallite growth, movement of the iron to the particles will expose the now Ir-rich alloy underlayer and start the evolution of a methanol-active surface. Slow diffusion of iron out of the alloy and slow sintering of the iron carbide phase can account for the 50-h time period required to reach maximum activity. Furthermore, the slow growth of the carbide phase could cause it to be carbon-poisoned before it can add significantly to the methane production. Both EXAFS and Mössbauer studies confirm that the alloy is Ir-rich in the active catalyst, in support of this model. Passivation and rereduction of the catalyst would lead, in this picture, to conversion of the iron carbide to iron metal. Thus, both the larger Fe particles, which were previously carbon-poisoned, and the smaller methane-active iron carbide particles will begin making methane when the reaction gas is reintroduced. The large particles, now perhaps more prominent because they include iron scavenged from the alloy, would go through the characteristic maximum and decay and account for the increase and relaxation of the methane yield seen in Fig. 1. The fact that the methanol yield restarts at the high value implies that the reduction does not remix the alloy or cause the iron to re-wet the Ir-rich alloy surface. This suggests that the iron extracted from the alloy moves off the alloy surface during the activation period.

CO bonding and hydrogenation activity. The ethylene hydrogenation experiments in (26) suggest that a clear correlation exists between the selectivity of the catalysts for methanol formation and their activity for ethylene hydrogenation in the presence of CO. The fresh 1 : 1 FeIr/SiO_2 catalyst has a low activity both for methanol synthesis and for ethylene hydrogenation. After activation, however, when the 1 : 1 FeIr catalyst has reached its favorable activity for methanol production, it is also significantly more active for ethylene hydrogenation. Interestingly, the fresh 1 : 5 FeIr/SiO_2 catalyst, with its high initial activity for methanol (4) also has an initially high hydrogenation activity. The Ir/SiO_2 catalyst is the least active in both methanol synthesis and ethylene hydrogenation, both after initial reduction and prolonged use in CO hydrogenation. Thus, the surface active for methanol synthesis is capable of hydrogenating ethylene in the presence of CO. As ethylene hydrogenation (in the absence of CO) occurs readily on most group-8 metals, we believe that the hydrogenation activity of the FeIr catalysts is associated with the adsorption strength of CO and thus with the extent that hydrogenation is poisoned by adsorbed CO. Support for this view is provided by the CO desorption studies as reported in (26).

The infrared experiments of Ref. (26) show that the increased hydrogenation activity of the activated FeIr/SiO_2 catalyst is accompanied by a significantly weakened adsorption strength of CO. These results thus suggest that Ir or FeIr surfaces modified, such that they adsorb CO only weakly, have a relatively high activity for hydrogenation, which is favorable for the formation of methanol from CO. We therefore propose that methanol formation occurs from a CO that is adsorbed on a monometallic iridium site, modified by the presence of iron. The promoting effect of the latter is attributed to a weakening of the Ir–CO bondstrength, resulting in an increased hydrogen coverage and higher hydrogenation capacity of the promoted surface. In this respect, the fact that a freshly reduced 1 : 5 FeIr/SiO_2 catalyst is active for methanol formation from the beginning of the CO hydrogenation, strongly suggests that an optimum composition of the alloy surface exists. The long period needed for activation of the 1 : 1 FeIr/SiO_2 which is accompanied by segregation and carburization of excess iron on the one hand and by achievement of a improved Fe–Ir mixing on the other, appears as an evolution to a catalyst that is optimally suited for methanol production.

CONCLUDING REMARKS

This work demonstrates that bimetallic catalysts such as 1 : 1 FeIr/SiO_2 may exhibit significant reorganizations in structure during high pressure CO hydrogenation which accompany a shift in activity and selectivity from production of hydrocarbons at the start of the reaction to production of methanol under steady state conditions. The main changes appear to be associated with the iron in the catalyst. We note that an FeIr catalyst with less iron and the same amount of iridium (Fe : Ir = 1 : 5) was active for methanol production from the beginning (4). This suggests that in fact the 1 : 1 FeIr catalyst contains more iron than favorable for methanol formation. It is interesting that during the first 24 to 48 h of CO hydrogenation, the 1 : 1 FeIr catalyst restructures to a more favorable composition for methanol production, by a process involving segregation, carburization and presumably deactivation by carbon deposition of the excess iron.

Figure 11 shows a model for the structure of 1 : 1 FeIr/SiO_2 after reduction and after activation of the catalyst in syngas at 275°C. After reduction the catalyst contains

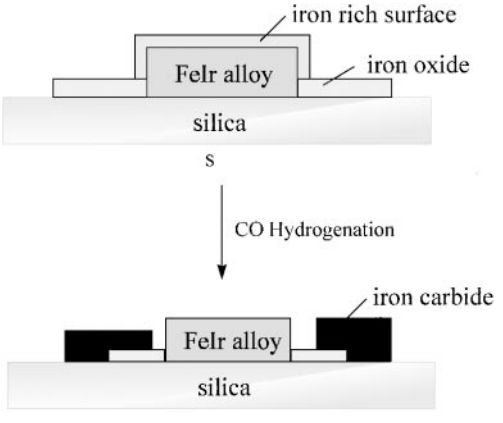

FIG. 11. Structure of the 1 : 1 FeIr/SiO_2 catalyst after reduction and exposure to CO (a), and during activation in high pressure synthesis gas.

predominantly FeIr alloy with a surface enriched in iron and well-dispersed iron oxide. CO hydrogenation induces iron to segregate to a large extent from the alloy after which iron carbide forms, which probably does not contribute to CO conversion (although it may still activate hydrogen). At the same time the overall degree of reduction increases, which we attribute to the high CO partial pressure. Carbonaceous species are deposited on the metal surface during reaction at temperatures above 150°C. The observed changes in surface structure are accompanied by weaker CO adsorption which is reflected by an increased activity of the catalyst for hydrogenation of ethylene in the presence of CO.

Overall, this work reveals two characteristics common to many supported catalyst systems: complexity and sensitivity to environment. Each of the measurements made shows clearly that the working catalyst is chemically and structurally different from the fresh catalyst, reiterating the well-known need for *in situ* characterization. Furthermore, the multitechnique approach used here shows both the need for a variety of views of the system and its complexity. In this case, the combination of surface and bulk information supplied by TPR, FTIR of CO, EXAFS, and Mössbauer spectroscopy rules out a number of simple explanations of the catalytic behavior and allows construction of a model that describes all observations. The fact that even this array of techniques is insufficient to identify the active site on a truly molecular scale is a reminder of the difficulty of achieving that goal.

REFERENCES

1. Bhasin, M. M., Bartley, W. J., Ellgen, P. C., and Wilson, T. P., *J. Catal.* **54**, 120 (1978).
2. Fukushima, T., Ishii, Y., and Ichikawa, M., *J. Chem. Soc., Chem. Commun.*, 1752 (1985).
3. Fukushima, T., Araki, K., and Ichikawa, M., *J. Chem. Soc., Chem. Commun.*, 148 (1986).
4. Koningsberger, D. C., Borgmans, C. P. J. H., Van Elderen, A. M. J., Kip, B. J., and Niemantsverdriet, J. W., *J. Chem. Soc., Chem. Commun.*, 892 (1987).
5. Niemantsverdriet, J. W., Louwers, S. P. A., Van Grondelle, J., Van Der Kraan, A. M., Kampers, F. W. H., and Koningsberger, D. C., *in* "Proceedings, 9th International Congress on Catalysis, 1988," Vol. 2, p. 674.
6. Garten, R. L., and Sinfelt, J. H., *J. Catal.* **62**, 127 (1980).
7. Guczi, L., *Catal. Rev.-Sci. Eng.* **23**, 329 (1981).
8. Van't Blik, H. F. J., and Niemantsverdriet, J. W., *Appl. Catal.* **10**, 155 (1984).
9. Niemantsverdriet, J. W., Van Der Kraan, A. M., and Delgass, W. N., *J. Catal.* **89**, 138 (1984).
10. Niemantsverdriet, J. W., Aschenbeck, D. P., Fortunato, F. A., and Delgass, W. N., *J. Molec. Catal.* **25**, 285 (1984).
11. Niemantsverdriet, J. W., Van Kaam, J. A. C., Flipse, C. F. J., and Van Der Kraan, A. M., *J. Catal.* **96**, 58 (1985).
12. Niemantsverdriet, J. W., and Van Der Kraan, A. M., *Surf. Interface Anal.* **9**, 221 (1986).
13. Ichikawa, M., Fukushima, T., Yokoyama, T., Kosugi, N., and Kuroda, H., *J. Phys. Chem.* **7**, 1222 (1986).
14. Martens, J. H. A., Prins, R., and Niemantsverdriet, J. W., *J. Catal.* **108**, 259 (1987).
15. Gatte, R. R., and Phillips, J., *J. Phys. Chem.* **91**, 5961 (1987).
16. Berry, F. J., and Jobson, S., *Hyperfine Interact.* **41**, 613 (1988).
17. Niemantsverdriet, J. W., Van Grondelle, J., and Van Der Kraan, A. M., *Hyperfine Interact.* **41**, 677 (1988).
18. Lietz, G., Nimz, M., Volter, J., Lazar, K., and Guczi, L., *Appl. Catal.* **45**, 71 (1988).
19. Woo, H. S., Fleisch, T. H., Foley, H. C., Uchiyama, S., and Delgass, W. N., *Catal. Lett.* **4**, 93 (1990).
20. Fukuoka, A., Kimura, T., Kosugi, N., Kuroda, H., Minai, Y., Sakai, Y., Tominaga, T., and Ichikawa, M., *J. Catal.* **126**, 434 (1990).
21. Ichikawa, M., Rao, L., Kimura, T., and Fukuoka, A., *J. Molec. Catal.* **62**, 15 (1990).
22. Kannan, K. R., Kulkarni, G. U., and Rao, C. N. R., *Catal. Lett.* **14**, 149 (1992).
23. Schuenemann, V., Trevino, H., Sachtler, W. M. H., Fogash, K., and Dumesic, J. A., *J. Phys. Chem.* **99**, 1317 (1995).
24. Schuenemann, V., Trevino, H., Lei, G. D., Tomczak, D. C., Sachtler, W. M. H., Fogash, K., and Dumesic, J. A., *J. Catal.* **153**, 144 (1995).
25. Marengo, S., Psaro, R., Dossi, C., Calmotti, S., and Della Pergola, R., *in* "Proceedings, 11th Int. Cong. Catal., Stud. Surf. Sci. Catal. Vol. 101" (J. W. Hightower, W. N. Delgass, E. Iglesia, and A. T. Bell, Eds.), p. 1411, Elsevier, Amsterdam, 1996.
26. Van Gruijthuisen, L. M. P., Louwers, S. P. A., Van Santen, R. A., and Niemantsverdriet, J. W., *Catal. Lett.* **43**, 45 (1997).
27. Bødker, F., Mørup, S., and Niemantsverdriet, J. W., *Catal. Lett.* **13**, 195 (1992).
28. Bødker, F., Mørup, S., Oxborrow, C. A., Linderoth, S., Madsen, M. B., and Niemantsverdriet, J. W., *J. Phys: Condens. Matt.* **4**, 6555 (1992).
29. Raupp, G. B., and Delgass, W. N., *J. Catal.* **58**, 348 (1979).
30. Niemantsverdriet, J. W., van der Kraan, A. M., van Dijk, W. L., and van der Baan, H. S., *J. Phys. Chem.* **84**, 3363 (1980).
31. Dry, M. E., *in* "Catalysis, Science and Technology, Vol. 1, p. 159" (J. R. Anderson and M. Boudart, Eds.), Springer-Verlag, Berlin, 1981.
32. Van't Blik, H. F. J., Van Zon, J. B. A. D., Huizinga, T., Vis, J. C., Koningsberger, D. C., and Prins, R., *J. Am. Chem. Soc.* **107**, 3139 (1985).
33. Mizushima, T., Tohji, K., Udagawa, Y., and Ueno, A., *J. Am. Chem. Soc.* **112**, 7887 (1990).
34. Solymosi, F., Novak, E., and Molnar, A., *J. Phys. Chem.* **94**, 7250 (1990).
35. Delgass, W. N., Haller, G. L., Kellerman, R., and Lunsford, J. H., "Spectroscopy in Heterogeneous Catalysis," Academic Press, New York, 1979.
36. Koningsberger, D. C., and Prins, R. (Eds.), "X-ray Absorption," Wiley, New York, 1987.
37. Niemantsverdriet, J. W., "Spectroscopy in Catalysis," VCH, Weinheim, 1993.
38. Teo, B. K., and Lee, P. A., *J. Am. Chem. Soc.* **101**, 2815 (1979).
39. Duivenvoorden, F. B. M., Koningsberger, D. C., Uh, Y. S., and Gates, B. C., *J. Am. Chem. Soc.* **108**, 6254 (1986).
40. Kampers, F. W. H., Engelen, C. W. R., van Hooff, J. H. C., and Koningsberger, D. C., *J. Phys. Chem.* **94**, 8574 (1990).
41. Mustre de Leon, J., Rehr, J. J., Zabinsky, S. I., and Albers, R. C., *Phys. Rev. B* **44**, 4146 (1991).
42. Vaarkamp, M., Dring, I., Oldman, R. J., Stern, E. A., and Koningsberger, D. C., *Phys. Rev. B* **50**, 7872 (1994).
43. Mössbauer, R. L., Lengsfeld, M., Von Lieres, W., Potzel, W., Teschner, P., Wagner, F. E., and Kaindl, G., *Z. Naturforsch.* **26**, 343 (1971).
44. Van Gruijthuijsen, L. M. P., Ph.D. thesis, Eindhoven University of Technology, 1993.
45. Vaarkamp, M., Miller, J. T., Modica, F. S., and Koningsberger, D. C., *J. Catal.* **163**, 294 (1996).
46. Amelse, J. A., Butt, J. B., and Schwartz, L. H., *J. Phys. Chem.* **82**, 558 (1978).
47. Jung, H.-J., Walker, P. L., and Vannice, M. A., *J. Catal.* **75**, 416 (1982).
48. Jung, H.-J., Vannice, M. A., Mulay, L. N., Stanfield, R. M., and Delgass, W. N., *J. Catal.* **76**, 208 (1982).